Acta Crystallographica Section D
Biological Crystallography
ISSN 1399-0047

Structure of an unusual *S*-adenosylmethionine synthetase from *Campylobacter jejuni*

Stephen P. Zano, Alexander G. Pavlovsky and Ronald E. Viola*

Department of Chemistry, The University of Toledo, Toledo, OH 43606, USA

Correspondence e-mail: ron.viola@utoledo.edu

Received 16 July 2013
Accepted 4 November 2013

PDB reference: *S*-adenosylmethionine synthetase, 4le5

S-Adenosylmethionine (AdoMet) participates in a wide range of methylation and other group-transfer reactions and also serves as the precursor for two groups of quorum-sensing molecules that function as regulators of the production of virulence factors in Gram-negative bacteria. The synthesis of AdoMet is catalyzed by AdoMet synthetases (MATs), a ubiquitous family of enzymes found in species ranging from microorganisms to mammals. The AdoMet synthetase from the bacterium *Campylobacter jejuni* (*cj*MAT) is an outlier among this homologous enzyme family, with lower sequence identity, numerous insertions and substitutions, and higher catalytic activity compared with other bacterial MATs. Alterations in the structure of this enzyme provide an explanation for its unusual dimeric quaternary structure relative to the other MATs. Taken together with several active-site substitutions, this new structure provides insights into its improved kinetic properties with alternative substrates.

1. Introduction

S-Adenosylmethionine (AdoMet), a sulfonium compound, is the major biological methyl donor and can also serve as a source of methylene, amino, ribosyl and aminopropyl groups in the metabolism of most species (Fontecave *et al.*, 2004). AdoMet donates its *S*-methyl group in the methylation of DNA, RNA, proteins and small molecules such as phospholipids and various neurotransmitters (Fontecave *et al.*, 2004). The methionine amino group of AdoMet is also donated in biotinylation reactions catalyzed by DAPA synthase (Stoner & Eisenberg, 1975). The ribosyl group of AdoMet is subsequently used in the biosynthesis of modified tRNA nucleosides (Van Lanen *et al.*, 2003), and the 5′-deoxyadenosyl moiety of AdoMet is involved in radical reactions that include the biosynthesis of deoxyribonucleotides and glycyl radical-generating reactions (Marsh *et al.*, 2010). Finally, AdoMet is a donor of aminopropyl groups to produce diamines during polyamine biosynthesis (Bowman *et al.*, 1973). In addition to these essential functions, AdoMet can also serve as the precursor for two different families of quorum-sensing molecules that trigger virulence in Gram-negative human pathogenic bacteria (Parsek *et al.*, 1999; Wei *et al.*, 2011; Galloway *et al.*, 2011).

The biosynthesis of AdoMet from L-methionine and ATP is exclusively catalyzed by *S*-adenosylmethionine synthetase or methionine adenosyltransferase (MAT; EC 2.5.1.6). MATs require two divalent metal ions (Mg^{2+}) in the active site in the presence of ATP for enzyme activity (Cantoni, 1975; Sánchez-Pérez *et al.*, 2004), and the addition of a single monovalent

cation such as K^+ stimulates catalytic activity (Markham *et al.*, 1980).

Sequence homologies among MATs demonstrate that it is a highly conserved cytosolic enzyme within eukarya and prokarya (Kotb & Geller, 1993; Cantoni, 1975; Sánchez-Pérez *et al.*, 2004) composed of 380–400 amino-acid residues. Five amino-acid clusters of high sequence preservation have been identified among the MAT family, including a methionine-binding motif, an ATP-binding motif and a characteristic pyrophosphate-recognition sequence for many MATs (Reczkowski *et al.*, 1998). The differences among the MAT sequences are confined to several inserts and deletions that occur in the loops connecting the secondary-structural elements of the protein (Sánchez-Pérez *et al.*, 2004).

The different orthologs of MATs primarily exist as homotetramers that assemble as dimers of dimers. However, some MATs from divergent classes, such as archaeal and mammalian MAT III isoforms, were found to exist as dimers in solution (Markham & Pajares, 2009). In addition, recombinant rat liver MAT was found in two oligomeric forms, dimer and tetramer, that exist in equilibrium and have been suggested to serve as a regulatory mechanism (Mingorance *et al.*, 1997).

The important position of AdoMet in a wide range of biological processes made the enzymes that are involved in its synthesis and utilization attractive targets for drug development. Of particular interest has been the blocking of the bacterial quorum-signaling pathway through altered AdoMet metabolism. Recently, we have identified structural analogs of the methionine substrate of several bacterial MATs with the potential to block quorum sensing while still serving as precursors for the essential methyl-donation reactions (Zano *et al.*, 2013). The MAT from *Campylobacter jejuni* (*cj*MAT) is an outlier among the sequences of MATs, with less than 40% sequence identity and numerous insertions and deletions compared with the other members of this homologous enzyme family. In addition, this isoenzyme has been shown to have a unique dimeric structure compared with the traditional homotetrameric oligomeric form of MATs. This enzyme form has also been found to have higher catalytic efficiency than the other bacterial MATs studied and possesses an altered substrate profile with different methionine derivatives (Zano *et al.*, 2013).

This current work reports the structure of this unusual form of MAT from *C. jejuni* (*cj*MAT). From an examination of this structure, assignments have been made of the key active-site functional groups, and new insights are provided into the observed substrate specificity and the unusual dimeric structure of this form of MAT.

2. Materials and methods

2.1. Materials and bacterial strains

All buffers, reagents, substrates and growth media were of the highest purity available from commercial sources. DNA polymerase and restriction enzymes were acquired from New England Biolabs, while plasmid Miniprep kits and gel-extraction kits were from Qiagen. The Champion pET Directional TOPO Expression Kit was acquired from Invitrogen. The cloning host TOP10 and expression host *Escherichia coli* BL21(DE3) competent cells were obtained from Invitrogen. The coupling enzymes and substrates used for the enzyme-activity assay were obtained from Sigma–Aldrich. Chromatography resins were acquired from GE Healthcare Life Sciences. The crystallization screening kit was obtained from Jena Bioscience and crystallization precipitants and additives were from Hampton Research.

2.2. Cloning, expression and enzyme purification

The experimental details regarding the cloning, expression and purification of *S*-adenosylmethionine synthetases have been described previously (Zano *et al.*, 2013). Briefly, the open reading frame of the *metK* gene of *C. jejuni* strain 81-176 was cloned into pET101/D-TOPO that introduces a C-terminal V5 epitope and hexahistidine tag. Positive clones were then transformed into the *E. coli* BL21(DE3) cell line and grown at 37°C to an OD_{600} of $\geq$0.75. Enzyme expression was then induced by adding 1 m*M* IPTG (isopropyl β-D-1-thiogalactopyranoside) and the culture was grown at 28°C for an additional 4 h. Cell paste was collected by centrifugation and the collected cell pellets were either used immediately or stored at −80°C until use.

5 g of cell paste was resuspended in 50 m*M* Tris–HCl pH 8.0, 300 m*M* KCl, 5 m*M* β-mercaptoethanol, 5% glycerol, 25 m*M* imidazole and sonicated. The clarified soluble lysate was loaded onto an Ni–IMAC column for the initial purification step. The active enzyme fractions were pooled and were further purified using a Source 30Q anion-exchange column on an ÄKTA chromatography system. Each step in the purification was monitored by SDS–PAGE.

2.3. Protein characterization

Approximately 1–2 µg of protein was electrophoresed and the bands were excised, in-gel reduced, alkylated, destained and proteolytically cleaved with trypsin following a standard protocol (Shevchenko *et al.*, 2006). Peptide mass maps were obtained by MALDI–TOF mass spectrometry using a Bruker ultrafleXtreme MALDI–TOF/TOF spectrometer, and the identity of the protein sample was confirmed by a *Mascot* database search (Perkins *et al.*, 1999).

2.4. Sequence alignment of AdoMet synthetases

Reference amino-acid sequences for the Gram-negative bacterial MATs were obtained from the UniProt database. Sequences were aligned using *ClustalW* v.2.0. A secondary-structure alignment of the sequences with the *E. coli* F11 structure (PDB entry 1rg9; Komoto *et al.*, 2004) was constructed using *ESPript* (Gouet *et al.*, 1999).

2.5. Protein crystallization and X-ray diffraction

Initial crystallization conditions were identified by sparse-matrix screening of *cj*MAT apoenzyme at a protein concentration of 10 mg ml^{-1} using JBScreen Basic (Jena Bioscience).

Table 1
Data-collection and refinement statistics.

Values in parentheses are for the highest resolution shell.

Data collection	
Wavelength (Å)	1.033
Space group	$P2_1$
Unit-cell parameters (Å, °)	a = 61.66, b = 113.10, c = 62.18, α = 90, β = 116.49, γ = 90
Resolution (Å)	50.0–1.7 (1.76–1.70)
Multiplicity	2.6 (2.1)
Completeness (%)	80.8 (72.2)
$R_{\rm merge}$ (%)	0.099 (0.577)
$\langle I/\sigma(I)\rangle$	17.8 (2.5)
No. of reflections	63467
Structure refinement	
$R_{\rm cryst}/R_{\rm free}$ (%)	22.5/25.7
R.m.s.d.s	
Bonds (Å)	0.008
Angles (°)	1.33
ESU based on $R_{\rm free}$ (Å)	0.15
No. of atoms (protein/water)	5975/191
Average B factor (Å^2)	39.9
Ramachandran plot, residues in† (%)	
Preferred regions	95.6
Allowed regions	3.5
Disallowed regions	0.9

† As reported by *Coot* (Emsley & Cowtan, 2004).

The optimized condition for the apoenzyme crystals consisted of 50 m*M* Tris–HCl pH 8.0, 200 m*M* KCl, 2% ethylene glycol, 1 m*M* DTT, 12–16% polyethylene glycol 8000. Small tetragonal prisms grew within 3–4 weeks of incubation at 13°C. The crystals diffracted to ∼2.2 Å resolution using an in-house R-AXIS IV image plate mounted on a Rigaku FR-E rotating-anode X-ray generator. Full crystallographic data were measured to 1.7 Å resolution on beamline 23ID-D of the GM/CA Collaborative Access Team at the Advanced Photon Source using a MAR Mosaic charge-coupled device detector with 16 tiled chips in a 4 × 4 array and a 300 × 300 mm sensitive area (MAR USA). *HKL*-2000 (Otwinowski & Minor, 1997) was used for indexing and integration and *SCALEPACK* was used for scaling the diffraction data. All statistical parameters for the data processing are summarized in Table 1.

2.6. Structure solution

The structure of *cj*MAT was determined by molecular replacement using *MOLREP* (Vagin & Teplyakov, 2010) in the *CCP*4 suite with the atomic coordinates of the monomer of *E. coli* MAT from the PDB (PDB entry 1rg9; Komoto *et al.*, 2004) as the probe. A single cycle of rigid-body refinement at 3.5 Å resolution using *REFMAC*5 (Murshudov *et al.*, 2011) was followed by restrained refinement at the highest resolution. At the last stage of refinement local NCS restraints were applied, which led to a decrease in the gap between $R_{\rm cryst}$ and $R_{\rm free}$, while slightly increasing $R_{\rm cryst}$. Revisions of the protein model and addition of water molecules were performed with *Coot* (Emsley & Cowtan, 2004). All peaks in the $2mF_{\rm o} - DF_{\rm c}$ map higher than 1σ and within hydrogen-bonding distance of polar protein atoms were examined using the water-placement procedure in *Coot*. The final structure was visualized and analyzed using either *VMD* (Humphrey *et al.*, 1996) or *PyMOL* (DeLano, 2002).

3. Results and discussion

3.1. Structural refinement

The structure of the AdoMet synthetase from *C. jejuni* (*cj*MAT) was refined to 1.7 Å resolution with a total of 191 water molecules bound per dimer. The final refinement statistics for this structure are summarized in Table 1.

The electron-density map allowed the building of residues 1–106 and 118–399 of monomer *A* and residues 1–111 and 124–398 of monomer *B*. Residues 107–117 of monomer *A* and residues 112–123 of monomer *B* were not built owing to a lack of interpretable electron density even at a lower contour level. These regions of the structure correspond to the *E. coli* MAT region that was previously shown to exist as a highly mobile element that was suggested to function as a dynamic lid over the substrate-binding site (Markham & Pajares, 2009). The V5 epitope and hexahistidine tag at the C-terminus of the enzyme are solvent-exposed and were also not built owing to a lack of electron density.

3.2. Overall structure and architecture of *cj*MAT

The asymmetric unit of *cj*MAT contains two monomers that are related by twofold symmetry and that represent the functional homodimer of the enzyme (Fig. 1*a*). This structural organization is in contrast to the other members of the MAT family from proteobacteria, which all exist as homotetramers. The *cj*MAT subunit structures consist of 398–399 residues, except for the 11–12-amino-acid region described above that is not visible in the electron-density map. Each domain of *cj*MAT is formed with the same secondary-structural topology as the other MAT structures, despite having only 38% sequence identity and multiple insertions in the sequence of the *cj*MAT gene. Similar to other MATs, the α-helices in each monomer of *cj*MAT are at solvent-exposed surfaces, while the hydrophobic β-sheets form the dimerization contact area in the quaternary structure of the enzyme. The two active-site pockets are formed primarily from amino acids on each of the monomers, oriented on the opposite sides of the dimeric structure.

The two monomers are nearly identical in overall structure, with the primary differences in the region of residues 110–124, the area of weak electron density that is proposed to act as an active-site lid. Many of the previously reported structures of MAT were also found to contain this disordered loop region. The exceptions are the structures with bound substrates (such as PDB entries 2po2 (Structural Genomics Consortium, unpublished work), 1p7l and 1rg9 (Komoto *et al.*, 2004), which have more ordered density for this loop, supporting its proposed role in controlling active-site access (Markham & Pajares, 2009). It has also been suggested that movement of this loop may be controlled by post-translational modification, such as nitrosylation (Castro *et al.*, 1999). However, such a modification would only be possible in the rat liver MAT

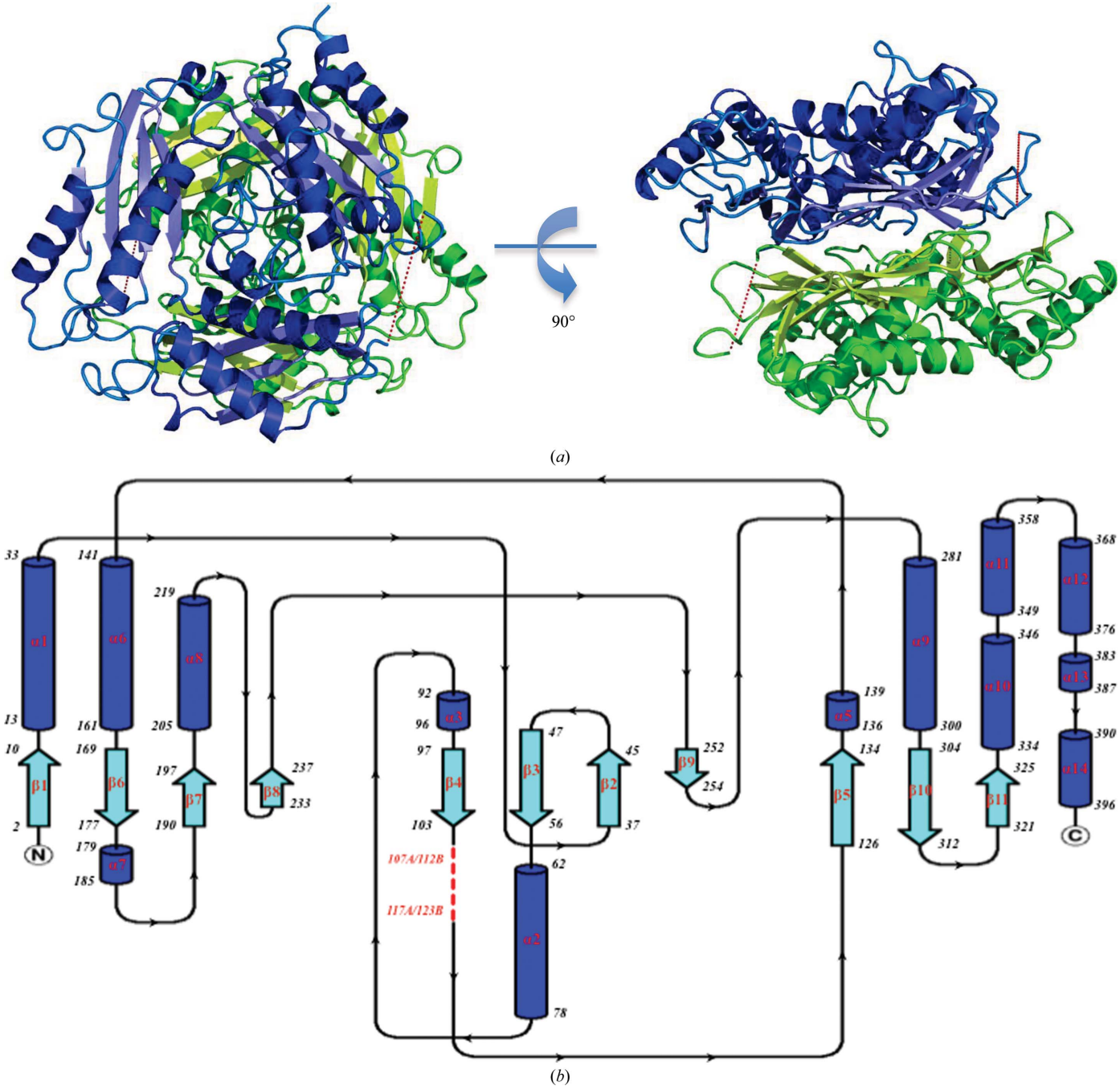

Figure 1
Overall structure of the dimeric *cj*MAT. (*a*) The two monomeric units are colored green and blue. The reported dynamic lid region that was not seen in this structure is indicated by a dashed red line in both subunits. (*b*) Topology map showing the secondary-structural organization of the *cj*MAT monomer, with the hydrophobic β-sheets that serve as the dimer interface colored cyan and the missing loop indicated by a dashed red line.

isoenzyme since this is the only member of the MAT family with a potentially modifiable cysteine residue (Cys105) in this region (Fig. 2) (Sánchez-Pérez *et al.*, 2004).

3.3. Secondary-structure comparison

Consistent with the classical MAT structure, *cj*MAT also belongs to the α/β protein class, with a $\beta\alpha\beta\beta\alpha\beta$ topology that is related to the Rossman fold found in many dehydrogenases (Markham & Pajares, 2009). The secondary structure of the N-terminus of *cj*MAT forms the roof of the substrate-binding site (Fig. 1*b*) and is similar to the other MAT structures. In the *E. coli* structure (*ec*MAT; PDB entry 1rg9), there is an α-helix (α2) followed by a short (2–5 amino acids in each secondary structure) $\beta\alpha\beta$ motif. However, this motif is instead a loop in *cj*MAT, while the loop in *ec*MAT found after this $\beta\alpha\beta$ motif is an α-helix in *cj*MAT. This region is then linked to a four-amino-acid β-strand (β4; seven amino acids in *ec*MAT) that forms a parallel β-sheet with β3.

Following the parallel β-strand β4 is the disordered loop that is proposed to serve as a dynamic lid that controls access

to the substrate-binding and active-site pocket (Markham & Pajares, 2009). This region was not modeled in each of the subunits owing to a lack of conclusive electron density even at very low contour levels. It is worth noting that the structure immediately before and after this missing region is positioned quite differently in subunits *A* and *B*, suggesting that this motif is also very mobile in *cj*MAT, thereby supporting the dynamic lid hypothesis. This region forms an α-helix in the *ec*MAT structure when the product AdoMet and the product analog PPNP are bound (Komoto *et al.*, 2004).

This disordered lid is linked to the next $\beta\alpha\beta\beta\alpha\beta$ motif in *ec*MAT. However, in *cj*MAT there is a seven-amino-acid insertion (residues 179–185) that forms an extra α-helix (α8) between β6 and β7, extending this motif to $\beta\alpha\beta\boldsymbol{\alpha}\beta\alpha\beta$ (Fig. 1*b*). This new α-helix is surface-exposed and is located ∼27 Å from the active site, on the opposite side of the dimer–dimer interface of the tetrameric assemblies found in the other microbial MATs. Information about the structure of the other characterized dimeric MAT, that from the archaeal bacterium *Methanococcus jannaschii* (*mj*MAT), is restricted to spectroscopic studies (Markham & Pajares, 2009). However, the observed differences in the circular-dichroism spectra (Lu & Markham, 2002) suggest that the secondary-structural topology of *mj*MAT contains significant differences compared with the classical MAT subunit (Graham *et al.*, 2000), and alignment of the *mj*MAT sequence with those of *ec*MAT and *cj*MAT shows very low sequence identity.

3.4. Active-site comparison

The clusters of active-site residues that are conserved among the MAT family members, including the methionine-binding motif (GHPDK), the ATP-binding motif (GAGDQG) and the characteristic pyrophosphate-recognition sequence (D*x*G*x*TGRKII) (Sánchez-Pérez *et al.*, 2004), are each well conserved in the *cj*MAT sequence (Zano *et al.*, 2013). The amino acids that are proposed to be involved in substrate binding in *ec*MAT are also the same in *cj*MAT, with only three exceptions: Tyr242, Asn244 and His249 (Fig. 3*a*). Phe230 in *ec*MAT has been reported to make a π–π stacking interaction with the adenine ring of the ATP substrate (Komoto *et al.*, 2004). The additional electron-withdrawing hydroxyl group at this position in the tyrosine (Tyr242) in *cj*MAT would decrease the strength of this interaction and could explain the twofold increase in K_m for ATP of *cj*MAT compared with *ec*MAT (Zano *et al.*, 2013). The G249H and I244N substitutions in *cj*MAT are likely to have a minimal effect on substrate binding since it is the backbone carbonyl groups at these positions that interact with the substrate through bound water molecules.

Electron density is not seen for AMPPNP in the *cj*MAT structure; however, superimposition with the *ec*MAT structure with AdoMet and PPNP bound shows that this region of *cj*MAT possesses the same pocket as the *ec*MAT active site. In addition, there are no significant differences in the organization of the active-site pocket formed in subunit *A* of *cj*MAT compared with that in *ec*MAT. In particular, Glu54, which interacts with the α-amino group of methionine, and the α-carboxyl binding groups (Gln105, Ser106 and Lys281) are each located in the same positions in the *cj*MAT active site (Fig. 3*a*). This suggests that the MAT active site is already preformed in the apoenzyme prior to substrate binding.

In contrast, in subunit *B* of *cj*MAT, in addition to the missing electron density for the active-site access loop, some of the active-site amino acids have significantly shifted positions relative to subunit *A*. The side chain of Thr239 that interacts with the adenine ring of ATP is shifted by ∼2.7 Å, and the

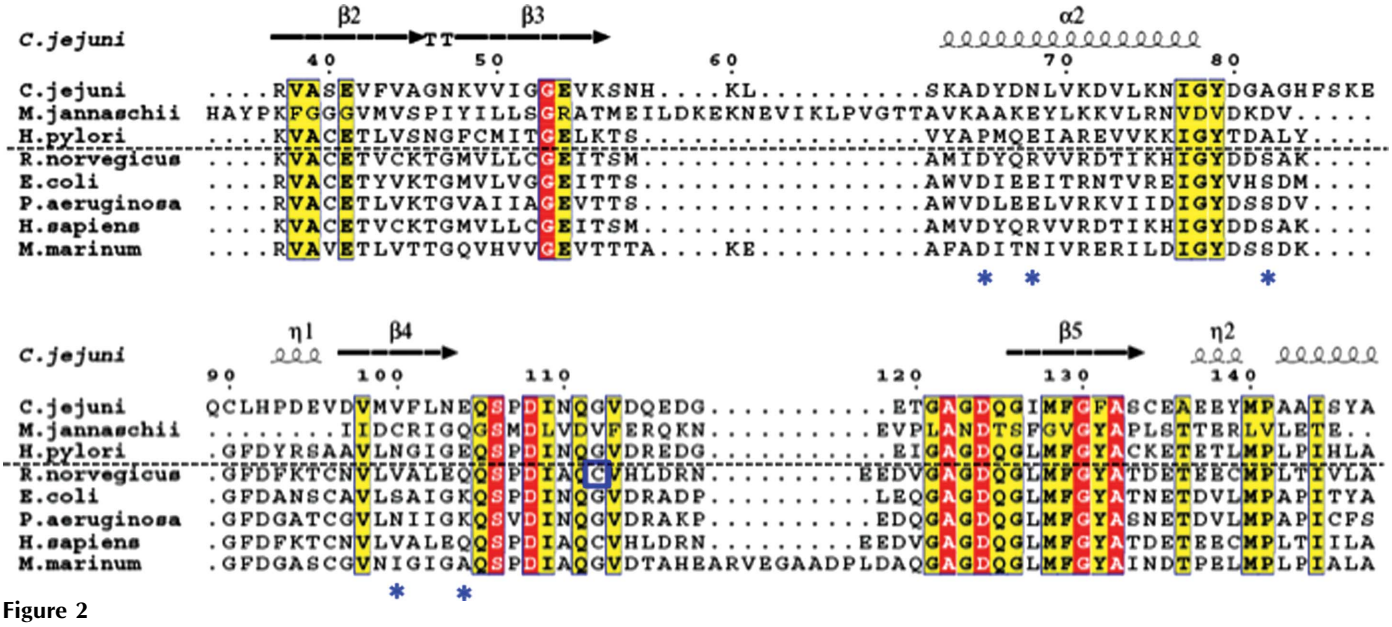

Figure 2
Sequence alignment of representative MAT enzymes showing the inserts and deletions between *cj*MAT and the other enzymes in this family. Fully conserved residues are shown in red boxes and residues with a single mutation among these MATs are shown in yellow boxes. Enzyme forms above the dashed line have dimeric structures. The residues that are involved in dimer–dimer interactions in the *ec*MAT tetrameric enzyme form are marked with blue asterisks and the cysteine involved in the disulfide linkage in dimer–dimer association of *rl*MAT is indicated by a blue box.

α-carboxyl binding groups Asn244, Gly123 and Ser106 are also shifted outwards by between 2 Å and nearly 10 Å (Fig. 3*b*). As a consequence, the active site in subunit *A* presents a more closed conformation that is consistent with substrate binding, while the active site in subunit *B* is in the more open conformation that would be required for product release. This asymmetry in active-site geometry suggests that an alternating-site mechanism is used by this dimeric form of MAT for the catalysis of AdoMet synthesis. While there is not any kinetic evidence suggesting such a mechanism, a similar increase in catalytic activity was observed between different orthologs of the enzyme ASA dehydrogenase. Kinetic evidence for an alternating-site mechanism of this enzyme was supported by the identification of a communication channel between the active sites in the functional enzyme dimer (Blanco *et al.*, 2003). Structural characterization of orthologs with low catalytic activity from *M. jannaschii* (Faehnle *et al.*, 2005) and *Candida albicans* (Arachea *et al.*, 2010) identified a disrupted communication channel in these enzyme forms. These observations support the catalytic advantage that can be achieved through active-site communication in each of the higher catalytic activity forms of ASA dehydrogenase and may offer an explanation for the higher catalytic activity of *cj*MAT.

3.5. The unusual dimeric structure of *cj*MAT

The consensus quaternary structure of the bacterial MATs is a homotetramer organized as a dimer of dimers, while each of the MAT isoenzymes from rat liver were shown to exist in a dimer–tetramer equilibrium, shifting between predominately dimeric (*rl*MAT III) and mainly tetrameric (*rl*MAT I) (Mato *et al.*, 1997). In contrast, evidence has been presented to show that *cj*MAT exists exclusively as a dimeric structure in solution (Zano *et al.*, 2013), similar to the reported structure of *mj*MAT from the divergent class of archaea (Lu & Markham, 2002). This newly determined high-resolution structure of *cj*MAT is consistent with the solution dimer. This unusual dimer of *cj*MAT is the first dimeric member of the MAT enzyme family that has been structurally characterized.

Similar to the predominant MAT structures, the subunit interface within the *cj*MAT dimer is formed by interactions across the flat hydrophobic surface of the β-sheet structure. The additional association of the dimers in both *ec*MAT and *rl*MAT to form the dimer of dimers also involves predominately hydrophobic contacts. Mapping of the hydrophilic/hydrophobic surface of the dimer–dimer association area of *ec*MAT using *UCSF Chimera* (Pettersen *et al.*, 2004) reveals the presence of a much larger hydrophobic surface compared with that in *cj*MAT (Fig. 4). This overall dimerization contact in *ec*MAT has been calculated to be 1800 Å^2 (Komoto *et al.*, 2004) and is composed predominately of a hydrophobic surface (Fig. 4*a*), while in *cj*MAT this hydrophobic surface area is significantly decreased (Fig. 4*b*). The more extensive hydrophobic contact surface in *ec*MAT would facilitate the formation of a highly stable tetrameric structure.

Rat liver MAT (*rl*MAT) is found in both dimeric and tetrameric forms, with each form possessing different kinetic

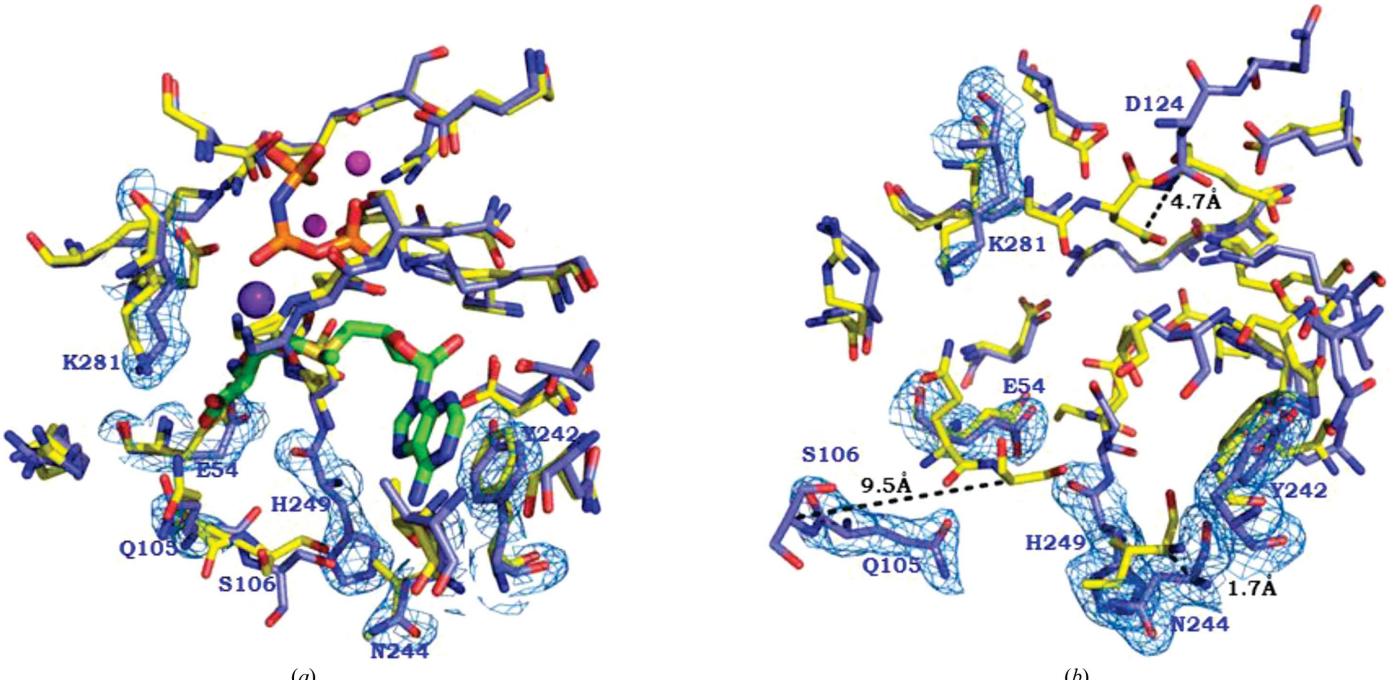

Figure 3
The active site of *cj*MAT (blue), showing the residues involved in substrate binding, superimposed with the active-site residues of *ec*MAT (yellow). The blue mesh indicates the electron density that was used to model the position of the *cj*MAT residues. (*a*) Residues of active site *A* of *cj*MAT are well aligned with residues from the *ec*MAT complex with bound substrates. Also shown for comparison are the AdoMet product (green) and PPNP product analog (orange) and two Mg^{2+} (magenta) and K^+ (purple) ions from the *ec*MAT structure. (*b*) Active site *B* of *cj*MAT showing the outward movement of the residues linked to the proposed dynamic lid of the active site.

and activation parameters, and shows different relative isoform levels during development (Mingorance *et al.*, 1997). Phosphorylation of *rl*MAT has been shown to alter its oligomeric state (Pajares *et al.*, 1994), suggesting a possible regulatory role. Interconversion of the *rl*MAT isoform between tetramer and dimer has also been shown to involve disulfide-bond formation in the dimer–dimer interaction (Sanchez-Perez *et al.*, 2003). However, the cysteines in each monomer of *cj*MAT are located remote from the dimer-interface region of MATs and cannot be involved in subunit association.

In addition to the central core of hydrophobic interactions, the *ec*MAT dimer–dimer contact is surrounded by a ring of additional contacts (Sanchez-Perez *et al.*, 2003). Examination of the *ec*MAT structure using *PyMOL* identified five amino acids from each monomer that are directly involved in dimer–dimer association (Fig. 4*a*, green surfaces). Sequence alignment reveals that these amino acids have been altered in the *cj*MAT structure. Ser82 in *ec*MAT, which hydrogen bonds to the corresponding Ser82 from the other subunit, is conserved in the other tetrameric MATs but has been replaced by an alanine (Ala82) in *cj*MAT (Fig. 2). The Ser100–Ser100 hydrogen-bonding interaction in *ec*MAT is disrupted by replacement with a valine at this position in *cj*MAT, but this serine interaction must not be as critical since this position is not conserved among the tetrameric MAT family. There is also an important electrostatic interaction between Lys104 in subunit *A* of *ec*MAT and the side-chain carboxyl groups of Asp65 and Asp68. In the mammalian MATs this interaction has been preserved, but its direction has been reversed. The positively charged amino acid is now found at position 68 in these enzyme forms and a polar amino acid has been substituted at position 104 (Fig. 2). While Asp65 is conserved in *cj*MAT, the glutamate at position 68 has been replaced by asparagine and the lysine at position 104 by a glutamate. These substitutions would lead to charge repulsion if two dimers from *cj*MAT attempted to associate in a similar orientation as observed in *ec*MAT. The surface of *cj*MAT also has a well distributed set of polar functional groups, especially in the region of the putative dimer–dimer association (Fig. 4*b*), in addition to the specific sequence and structural differences of *cj*MAT compared with other MATs. These features of *cj*MAT result in its unusual dimeric structure.

3.6. Structure–activity comparisons

*cj*MAT has been shown to possess differences in substrate specificity and in catalytic activity compared with its MAT counterparts from *E. coli*, *Neisseria meningitidis* and *Pseudomonas aeruginosa* (Zano *et al.*, 2013). *cj*MAT has a threefold to fourfold higher catalytic efficiency (V_{max}/K_m) compared with its bacterial counterparts. This higher activity appears to be a consequence of the unusual dimeric form of *cj*MAT. This enzyme form presents a more open and accessible active site compared with its tetrameric counterpart since the dimer–dimer interface of classical MATs is situated between the two active sites of each MAT dimer.

Structural characterization of the bacterial forms of AdoMet synthetases will provide a basis to guide the synthesis and testing of alternative substrates that will lead to modified forms of AdoMet. The goal is to develop AdoMet analogs that can function in the full range of essential mammalian activities while being incapable of conversion to quorum-signaling molecules that trigger virulence responses. Screening of the recombinant MATs for alternative substrates found that

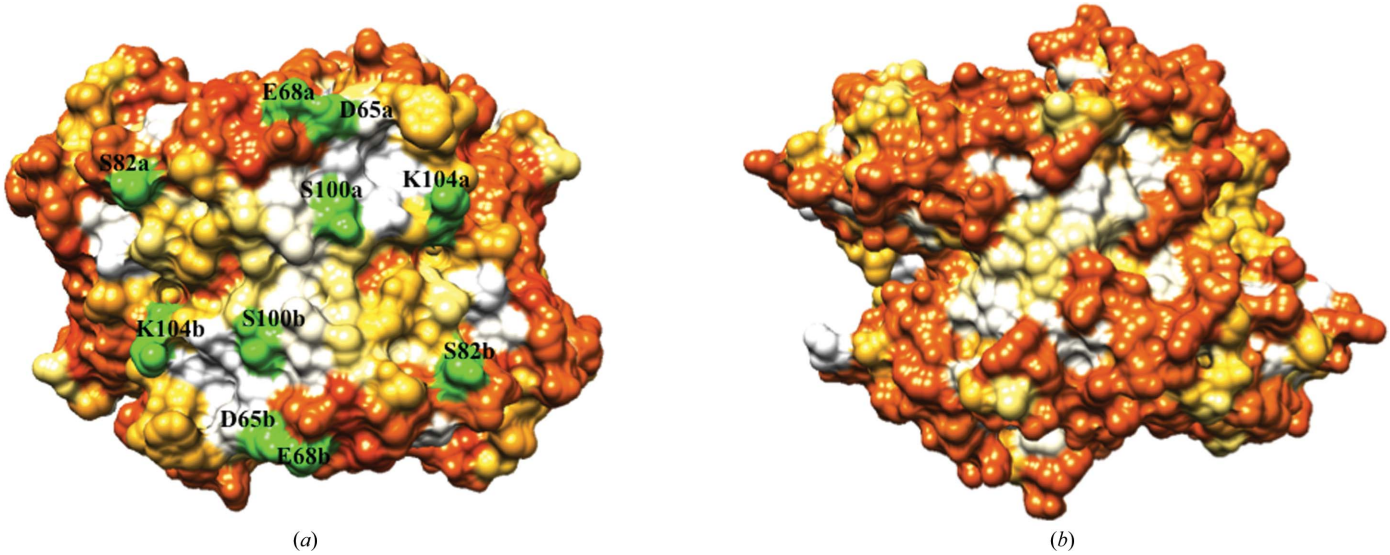

Figure 4
Hydrophobicity surface map of the dimer–dimer association region of *ec*MAT in comparison to the same region in *cj*MAT. The orange-shaded regions are the most hydrophilic surfaces, shifting through yellow to white from the least to the most hydrophobic surfaces. The amino acids that are labeled and highlighted in green are involved in direct binding interactions across the dimer–dimer boundary. (*a*) *ec*MAT showing the dimerization binding surface. The associated dimer would be rotated by 180° around the *x* and *y* axes to allow complementary hydrogen bonding between the Ser82 and Ser100 pairs of amino acids (*cj*MAT numbering). (*b*) *cj*MAT showing the same differences in the potential dimerization binding surface. Hydrophobic maps were generated using *UCSF Chimera* (Pettersen *et al.*, 2004).

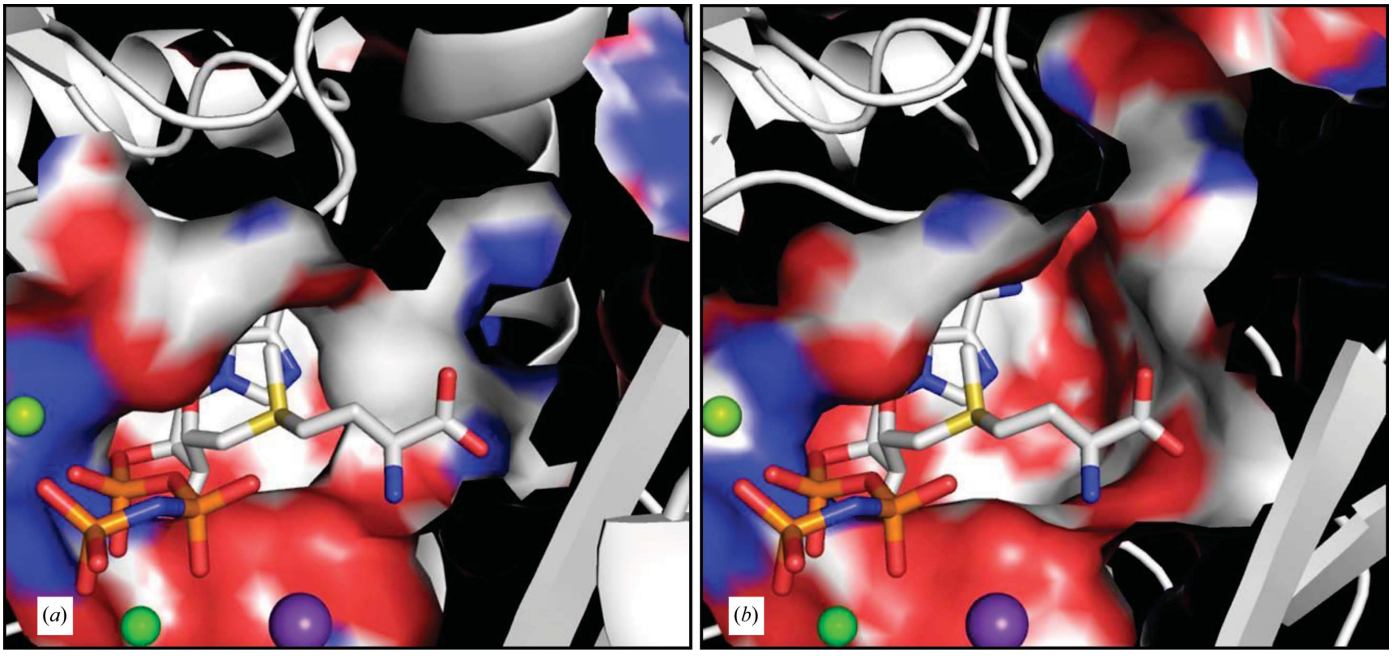

Figure 5
Comparison of the methionine substrate-binding pocket between *ec*MAT and *cj*MAT, showing the additional space available in the *cj*MAT structure that allows the binding of bulkier esters. (*a*) The more constrained binding pocket in *ec*MAT. (*b*) The more open pocket to accommodate bulkier methionine esters in *cj*MAT.

*cj*MAT has a different profile to those of the other forms of MAT that were examined (Zano *et al.*, 2013). Unlike the other bacterial MATs, the *cj*MAT enzyme shows enhanced activity with increasing size of the ester derivatives of L-methionine compared with *ec*MAT. We had previously speculated that the P267Y substitution in *cj*MAT would disrupt the substrate carboxyl-binding pocket and allow accommodation of the bulky ester derivatives. However, upon examination of the *cj*MAT structure this alteration causes only a modest change in the substrate-binding pocket. Instead, the unique dimeric structure of *cj*MAT exposes the parallel β-sheets that are normally involved in the dimer–dimer association in the bacterial MAT enzymes. In addition, these β-strands (β3 and β4) are shorter in *cj*MAT, with the additional amino acids assigned as loops. As a consequence, the constrained carboxyl-binding pocket in *ec*MAT (Fig. 5*a*) is more open in *cj*MAT (Fig. 5*b*), which would serve to accommodate the bulkier ester derivatives of L-methionine.

References

Arachea, B. T., Liu, X., Pavlovsky, A. G. & Viola, R. E. (2010). *Acta Cryst.* D**66**, 205–212.
Blanco, J., Moore, R. A., Kabaleeswaran, V. & Viola, R. E. (2003). *Protein Sci.* **12**, 27–33.
Bowman, W. H., Tabor, C. W. & Tabor, H. (1973). *J. Biol. Chem.* **248**, 2480–2486.
Cantoni, G. L. (1975). *Annu. Rev. Biochem.* **44**, 435–451.
Castro, C., Ruiz, F. A., Pérez-Mato, I., Sánchez del Pino, M. M., LeGros, L., Geller, A. M., Kotb, M., Corrales, F. J. & Mato, J. M. (1999). *FEBS Lett.* **459**, 319–322.
DeLano, W. L. (2002). *PyMOL*. http://www.pymol.org.
Emsley, P. & Cowtan, K. (2004). *Acta Cryst.* D**60**, 2126–2132.
Faehnle, C. R., Ohren, J. F. & Viola, R. E. (2005). *J. Mol. Biol.* **353**, 1055–1068.
Fontecave, M., Atta, M. & Mulliez, E. (2004). *Trends Biochem. Sci.* **29**, 243–249.
Galloway, W. R., Hodgkinson, J. T., Bowden, S. D., Welch, M. & Spring, D. R. (2011). *Chem. Rev.* **111**, 28–67.
Gouet, P., Courcelle, E., Stuart, D. I. & Métoz, F. (1999). *Bioinformatics*, **15**, 305–308.
Graham, D. E., Bock, C. L., Schalk-Hihi, C., Lu, Z. J. & Markham, G. D. (2000). *J. Biol. Chem.* **275**, 4055–4059.
Humphrey, W., Dalke, A. & Schulten, K. (1996). *J. Mol. Graph.* **14**, 33–38.
Komoto, J., Yamada, T., Takata, Y., Markham, G. D. & Takusagawa, F. (2004). *Biochemistry*, **43**, 1821–1831.
Kotb, M. & Geller, A. M. (1993). *Pharmacol. Ther.* **59**, 125–143.
Lu, Z. J. & Markham, G. D. (2002). *J. Biol. Chem.* **277**, 16624–16631.
Markham, G. D., Hafner, E. W., Tabor, C. W. & Tabor, H. (1980). *J. Biol. Chem.* **255**, 9082–9092.
Markham, G. D. & Pajares, M. A. (2009). *Cell. Mol. Life Sci.* **66**, 636–648.
Marsh, E. N., Patterson, D. P. & Li, L. (2010). *Chembiochem*, **11**, 604–621.
Mato, J. M., Alvarez, L., Ortiz, P. & Pajares, M. A. (1997). *Pharmacol. Ther.* **73**, 265–280.
Mingorance, J., Alvarez, L., Pajares, M. A. & Mato, J. (1997). *Int. J. Biochem.* **29**, 485–491.
Murshudov, G. N., Skubák, P., Lebedev, A. A., Pannu, N. S., Steiner, R. A., Nicholls, R. A., Winn, M. D., Long, F. & Vagin, A. A. (2011). *Acta Cryst.* D**67**, 355–367.
Otwinowski, Z. & Minor, W. (1997). *Methods Enzymol.* **276**, 307–326.
Pajares, M. A., Durán, C., Corrales, F. & Mato, J. M. (1994). *Biochem. J.* **303**, 949–955.
Parsek, M. R., Val, D. L., Hanzelka, B. L., Cronan, J. E. & Greenberg, E. P. (1999). *Proc. Natl Acad. Sci. USA*, **96**, 4360–4365.
Perkins, D. N., Pappin, D. J., Creasy, D. M. & Cottrell, J. S. (1999). *Electrophoresis*, **20**, 3551–3567.

Pettersen, E. F., Goddard, T. D., Huang, C. C., Couch, G. S., Greenblatt, D. M., Meng, E. C. & Ferrin, T. E. (2004). *J. Comput. Chem.* **25**, 1605–1612.
Reczkowski, R. S., Taylor, J. C. & Markham, G. D. (1998). *Biochemistry*, **37**, 13499–13506.
Sánchez-Pérez, G. F., Bautista, J. M. & Pajares, M. A. (2004). *J. Mol. Biol.* **335**, 693–706.
Sanchez-Perez, G. F., Gasset, M., Calvete, J. J. & Pajares, M. A. (2003). *J. Biol. Chem.* **278**, 7285–7293.
Shevchenko, A., Tomas, H., Havliš, J., Olsen, J. V. & Mann, M. (2006). *Nature Protoc.* **1**, 2856–2860.
Stoner, G. L. & Eisenberg, M. A. (1975). *J. Biol. Chem.* **250**, 4037–4043.
Vagin, A. & Teplyakov, A. (2010). *Acta Cryst.* D**66**, 22–25.
Van Lanen, S. G., Kinzie, S. D., Matthieu, S., Link, T., Culp, J. & Iwata-Reuyl, D. (2003). *J. Biol. Chem.* **278**, 10491–10499.
Wei, Y., Perez, L. J., Ng, W. L., Sempere, R. & Bassler, B. L. (2011). *ACS Chem. Biol.* **6**, 356–365.
Zano, S. P., Bhansali, P., Luniwal, A. & Viola, R. E. (2013). *Arch. Biochem. Biophys.* **536**, 64–71.